Journal of Magnetic Resonance 289 (2018) 45–54

Contents lists available at ScienceDirect

Journal of Magnetic Resonance

journal homepage: www.elsevier.com/locate/jmr

Frequency-agile gyrotron for electron decoupling and pulsed dynamic nuclear polarization

Faith J. Scott [a], Edward P. Saliba [a], Brice J. Albert [a], Nicholas Alaniva [a], Erika L. Sesti [a], Chukun Gao [a], Natalie C. Golota [a], Eric J. Choi [a], Anil P. Jagtap [b], Johannes J. Wittmann [c], Michael Eckardt [d,e], Wolfgang Harneit [d,e], Björn Corzilius [c], Snorri Th. Sigurdsson [b], Alexander B. Barnes [a,*]

[a] Department of Chemistry, Washington University in St. Louis, One Brookings Drive, St. Louis, MO 63130, USA
[b] Department of Chemistry, Science Institute, University of Iceland, Dunhaga 3, 107 Reykjavik, Iceland
[c] Institute for Physical and Theoretical Chemistry, Institute of Biophysical Chemistry, and Center for Biomolecular Magnetic Resonance (BMRZ), Goethe University Frankfurt, Max-von-Laue-Str. 7-9, 60438 Frankfurt am Main, Germany
[d] Institut für Physikalische Chemie, Johannes Gutenberg-Universität Mainz, Duesbergweg 10–14, 55099 Mainz, Germany
[e] Fachbereich Physik, Universität Osnabrück, Barbarastr. 7, 49076 Osnabrück, Germany

ARTICLE INFO

Article history:
Received 20 December 2017
Revised 9 February 2018
Accepted 11 February 2018
Available online 12 February 2018

Keywords:
Dynamic nuclear polarization
Electron decoupling
Gyrotron
Chirp pulses
Pulsed DNP

ABSTRACT

We describe a frequency-agile gyrotron which can generate frequency-chirped microwave pulses. An arbitrary waveform generator (AWG) within the NMR spectrometer controls the microwave frequency, enabling synchronized pulsed control of both electron and nuclear spins. We demonstrate that the acceleration of emitted electrons, and thus the microwave frequency, can be quickly changed by varying the anode voltage. This strategy results in much faster frequency response than can be achieved by changing the potential of the electron emitter, and does not require a custom triode electron gun. The gyrotron frequency can be swept with a rate of 20 MHz/μs over a 670 MHz bandwidth in a static magnetic field. We have already implemented time-domain electron decoupling with dynamic nuclear polarization (DNP) magic angle spinning (MAS) with this device. In this contribution, we show frequency-swept DNP enhancement profiles recorded without changing the NMR magnet or probe. The profile of endofullerenes exhibits a DNP profile with a <10 MHz linewidth, indicating that the device also has sufficient frequency stability, and therefore phase stability, to implement pulsed DNP mechanisms such as the frequency-swept solid effect. We describe schematics of the mechanical and vacuum construction of the device which includes a novel flanged sapphire window assembly. Finally, we discuss how commercially available continuous-wave gyrotrons can potentially be converted into similar frequency-agile high-power microwave sources.

1. Introduction

Dynamic nuclear polarization (DNP) is a powerful tool to increase nuclear magnetic resonance (NMR) sensitivity in which the high polarization of electron spins is transferred to nuclear spins via microwave irradiation that fulfills matching conditions [1–3]. High microwave power levels (>5 W) are required to generate significant DNP enhancements for magic angle spinning (MAS) samples at temperatures >80 K at high magnetic fields (>5 T) [4–6]. Gyrotrons, now widely commercially available, provide the requisite microwave power levels, yet can rarely be tuned quickly or pulsed [7]. Such continuous-wave (CW) gyrotrons permit only CW DNP mechanisms. Similar to the development of NMR and EPR spectroscopy from continuous wave to pulsed regimes, pulsed DNP will provide many advantages over CW approaches [8–12]. Although CW DNP mechanisms yield large signal enhancements for model systems at lower magnetic fields, their performance is sub-optimal with higher magnetic fields, higher temperatures, and more complex samples [13,14]. Pulsed DNP transfers have considerable promise to improve DNP performance where CW mechanisms under-perform [15–18]. Chirped microwave pulses have also recently enabled the first electron decoupling experiments, which attenuate hyperfine interactions and alleviate detrimental paramagnetic relaxation effects [8].

Possible microwave sources which can produce high power levels required for pulsed DNP and electron decoupling with MAS include free electron lasers, slow-wave traveling wave tubes

* Corresponding author.
E-mail address: barnesab@wustl.edu (A.B. Barnes).

https://doi.org/10.1016/j.jmr.2018.02.010
1090-7807/

(TWTs), gyromonotrons, gyro-TWTs, and gyro-backward wave oscillators (BWOs) [19–24]. Free electron lasers are unrivaled in their tuning range and can also be frequency and phase stable, yet occupy considerable volume making their broad applicability in NMR laboratories across the world limited [25]. Slow-wave TWTs are very promising sources for EPR and DNP below 300 GHz, yet their maximum power levels are lower than gyrotrons, and the inverse scaling of the interaction cavity dimensions with higher frequencies presents considerable micro-fabrication challenges [26,27]. Fast-wave gyro-TWTs have successfully been developed at 140 and 250 GHz, yet their broad dissemination into the ranks of NMR spectroscopists has been hindered by the cost associated with the requisite super-conducting magnets and electron beam power supplies [20,28–30]. We have chosen to instead focus on the development of frequency agile gyrotrons, which fall under the category of gyro-BWOs. Gyrotrons have numerous advantages including higher-power levels (up to 1 MW, 100% duty cycle) and possible widespread dissemination of technology through upgrades of existing and available MAS DNP spectrometers.

Gyrotrons are especially appealing due to the experimental feasibility of implementing chirped pulses for time-domain DNP and electron decoupling, rather than hard pulses which are more commonly employed in NMR spectroscopy of spin ½ nuclei. For instance, we previously calculated that 13 MW of microwave power are required to generate sufficient electron Rabi frequency (ω_{1e}) for a hard pulse to excite the 800 MHz nitroxide lineshape at 7 T, given current widely available MAS DNP probes [31]. Furthermore, the wavelength of high-frequency microwaves is smaller than the sample geometries currently employed in MAS DNP experiments leading to severe inhomogeneity of the electron Rabi frequency, and would lead to a concomitant poor performance of hard pulses. Notably, frequency chirped pulses such as adiabatic rapid passages remain effective with a high degree of ω_{1e} inhomogeneity [9,10]. Microwave resonance structures and focusing strategies (i.e. TE_{01} resonators and Teflon lenses) are being developed by our group and others, and could provide both uniform and intense ω_{1e} fields required for pulsed DNP. However, we note that their applicability will most likely be restricted to sample-limited applications, as larger samples currently provide higher sensitivity in MAS DNP experiments. Gyrotrons which exhibit fast frequency tuning, or pulsing, include those described by Idehara et al., Alberti et al., and the device we present herein [32–34]. In this paper we describe the mechanical, vacuum, and electrical design of a frequency-agile gyrotron which has previously been employed in pulsed electron decoupling experiments [8]. We also measure frequency swept DNP enhancement profiles of various polarizing agents using the gyrotron. Importantly, the DNP enhancement profiles of an endofullerene, $N@C_{60}$, indicate that the gyrotron has the frequency and phase stability required to perform time domain DNP transfers such as the integrated solid effect. Finally, we conclude with a discussion of how currently available spectrometers could possibly be upgraded to provide similar frequency agility and a concomitant acceleration of the field of MAS DNP into the pulsed regime.

2. Design

2.1. Overview

The gyrotron is shown within the context of the DNP-MAS NMR spectrometer (Fig. 1), of which many components were custom-built such as the NMR probe, cryostat, heat-exchanger, and corrugated waveguide transmission line. Corrugated transmission line transmits microwave power from the gyrotron to the NMR probe. A cryostat insulates the NMR superconducting magnet and facilitates cryogenic MAS <6 K [35,36]. The DNP NMR probe includes a four-channel transmission line circuit resonating at 300.184 MHz (^{1}H), 75.495 MHz (^{13}C), 30.427 MHz (^{15}N), and 121.516 MHz (^{31}P) [37,38]. A Tecmag Redstone spectrometer (Tecmag Inc., Houston TX), drives each channel and includes an arbitrary waveform generator (AWG) to generate shaped microwave pulses.

The potential waveform from the AWG is amplified 1000:1 by a low capacitance, high voltage Trek 5/80-L linear amplifier (Trek, Lockport, NY). The amplifier output is connected to the gyrotron anode, as shown in Fig. 2c and 3a. An electron beam is emitted from a magnetron injection gun (MIG), and compressed by the magnetic field gradient into the interaction cavity. A portion of the electron beam power is deposited into the TE_{52q} cylindrical resonator. Microwaves are directed out of the gyrotron by the internal mode converter while the electron beam continues up through the gyrotron body. Finally, the remaining electron beam energy is absorbed at the grounded collector.

2.2. Electrical isolation and frequency agility

The amplifier driven by the AWG is connected to the anode by a low-capacitance wire (pseudo-colored in yellow for clarity, Fig. 3a). This high-voltage wire is isolated to reduce stray circuit capacitance. The cathode, which emits the electron beam, is connected to a separate high-voltage, high-power (4 kW) supply (Fig. 2c and 3b) (Spellman, Hauppage, NY). Note that the capacitance of the cathode power supply is very large to maintain a stable potential, yet prevents the generation of quickly-swept microwave waveforms via control of only the cathode potential. The anode amplifier has a low power and voltage requirement which permits a fast slew rate of 1000 V/μs due to a low internal capacitance. Therefore the potential of the anode can be changed quickly and results in microwave output frequency agility of up to 20 MHz/μs. This allows for frequency jumps from the DNP matching condition to the electron spin resonance for electron decoupling [8,31], and should permit coherent electron spin manipulation with adiabatic chirped pulses.

Ceramic breaks allow for electrical isolation between different sections of the gyrotron (Fig. 2c). Vacuum ion pumps must be grounded to function properly and are electrically isolated from the collector and anode. The collector is also grounded so that the electron beam colliding with its surface does not accrue a negative charge. Note that the collector must be kept electrically separated from the anode to permit fast microwave frequency tuning.

The microwave output frequency is partially determined by the acceleration potential of electron emission. The electron beam is generated by a barium impregnated tungsten ring within the MIG and carries 190 mA of current. The potential between the anode and cathode is maintained between 9 and 17 kV. This high potential accelerates electrons to relativistic speeds. The associated increase in electron mass results in a lower microwave frequency according to the cyclotron frequency equation:

$$\Omega = \frac{eB_0}{m} \tag{1}$$

where Ω is the cyclotron resonance frequency, e is the charge of the electron, B_0 is the magnetic field at the interaction cavity, and m is the relativistic electron mass [24]. Within the interaction cavity the electron beam deposits power into a cylindrical microwave mode. This TE_{52q} mode supports a continuous tuning bandwidth over a frequency range of 197.2–198.4 GHz, which can be controlled with 1 MHz precision by adjusting the potential across the MIG. Here, the q subscript refers to axial modes present along the long axis of the cylindrical resonator (Fig. 4a) [7,22].

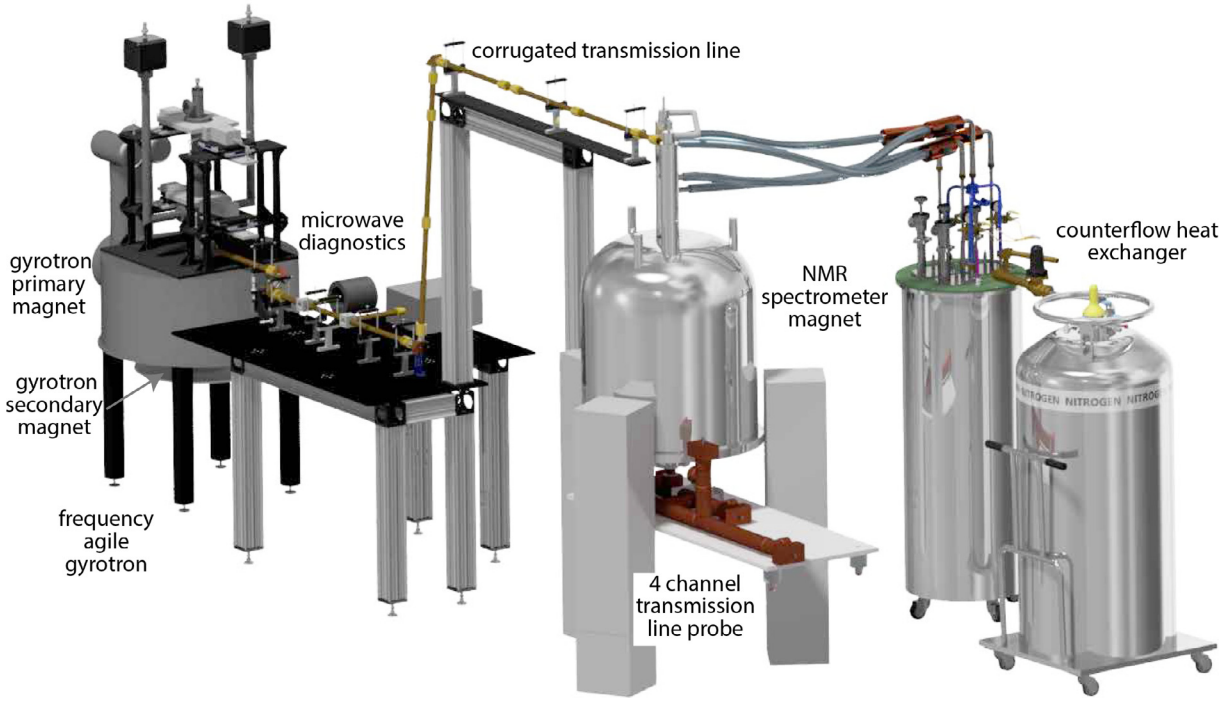

Fig. 1. Schematic of the DNP spectrometer showing the NMR magnet, probe, microwave transmission line, gyrotron, and heat exchanger.

2.3. Interaction cavity

The cavity radius is 2.542 mm, optimized for interaction with the electron beam. The magnetic field gradient focuses the electron beam at a compression factor of 28 for optimal overlap with the TE_{52q} mode [7]. The compression factor is defined as R_{MIG}/R_C where R_{MIG} is the beam radius at the MIG and R_C is the beam radius at the interaction cavity. Ohmic losses in the copper cavity walls generate heat. If the cavity is sufficiently heated, the cavity radius and frequency change concomitantly [39]. For this reason, the cavity is cooled by a water channel within the stainless steel outer jacket (Fig. 4c). The 30 mm long interaction cavity supports a large continuous frequency bandwidth, here explored from 197.2 GHz to 198.4 GHz to allow for electron paramagnetic resonance (EPR) or DNP excitation of several radicals. The cavity can support up to 0.67 GHz bandwidth for a fixed magnetic field, and the gyrotron can access additional frequency ranges by adjusting the primary gyrotron magnetic field. In this way, the gyrotron can excite EPR/DNP transitions for a variety of different radicals without changing the NMR spectrometer magnetic field.

Achieving continuous tuning of >1 GHz with gyrotrons requires access to hybridized axial modes within in the interaction cavity (Fig. 4a) [7,22]. Therefore, we used a cavity with a length of 30 mm (20 λ for 198 GHz electromagnetic radiation in a vacuum), which supports hybridized axial modes. After the straight section of the interaction cavity, the walls taper away from the center for 37 mm until the Vlasov launcher of the internal mode converter. The taper prevents parasitic oscillations as the beam expands in the weaker magnetic field above the interaction cavity.

2.4. Internal mode converter

The microwaves generated in the interaction cavity (Fig. 4b) propagate inside the gyrotron in the TE_{52q} mode, which is not supported by an overmoded corrugated transmission line [40]. For this reason, it is desirable to convert the microwave output into a beam of high Gaussian content which couples with high efficiency to the HE_{11} mode supported within the waveguide [7]. The TE_{52q} mode is broadcasted by a Vlasov launcher and further shaped by an off-axis parabolic mirror and three concave mirrors [24,41]. The Vlaslov launcher and mirrors are defined as the internal mode converter. All portions of the internal mode converter are machined in copper so that the microwaves can reflect off the surface in a quasi-optical manner. The internal mode converter is specifically designed for the TE_{52q} mode; other modes will not be converted efficiently into a Gaussian-like beam.

2.5. Interaction cavity and internal mode converter deficiencies

The ceramic break above the window reaches up to 82 °C during nominal operation despite plastic water cooling lines, as shown in Fig. 3a. This indicates that a portion of the microwave power is trapped inside the gyrotron body and absorbed into the ceramic break as heat. There are several possible reasons why microwaves may be misdirected inside the tube. First, mode excitation in the cavity may not be the expected TE_{52q} mode and is, therefore, not properly reflected by the mode converter. However the TE_{52q} mode was specifically chosen for operation because there are no competing modes nearby in frequency [7]. Second, a cylindrical section between the interaction cavity and the Vlasov launcher could act as a secondary cavity and generate microwaves in a competing mode. Third, gaps in the tapered waveguide between the cavity and the Vlasov launcher or misalignments in the interaction cavity could cause a significant portion of microwaves to be scattered away from the window. These potential sources of error will be addressed in the next generation of the frequency-agile gyrotron, currently under fabrication.

2.6. Output window

The microwave output port is a sapphire window cut perpendicular to the crystallographic C-axis, with a width of 0.0685 mm to optimally transmit 198 GHz microwaves. An incorrect window thickness would reflect the majority of the microwaves back into

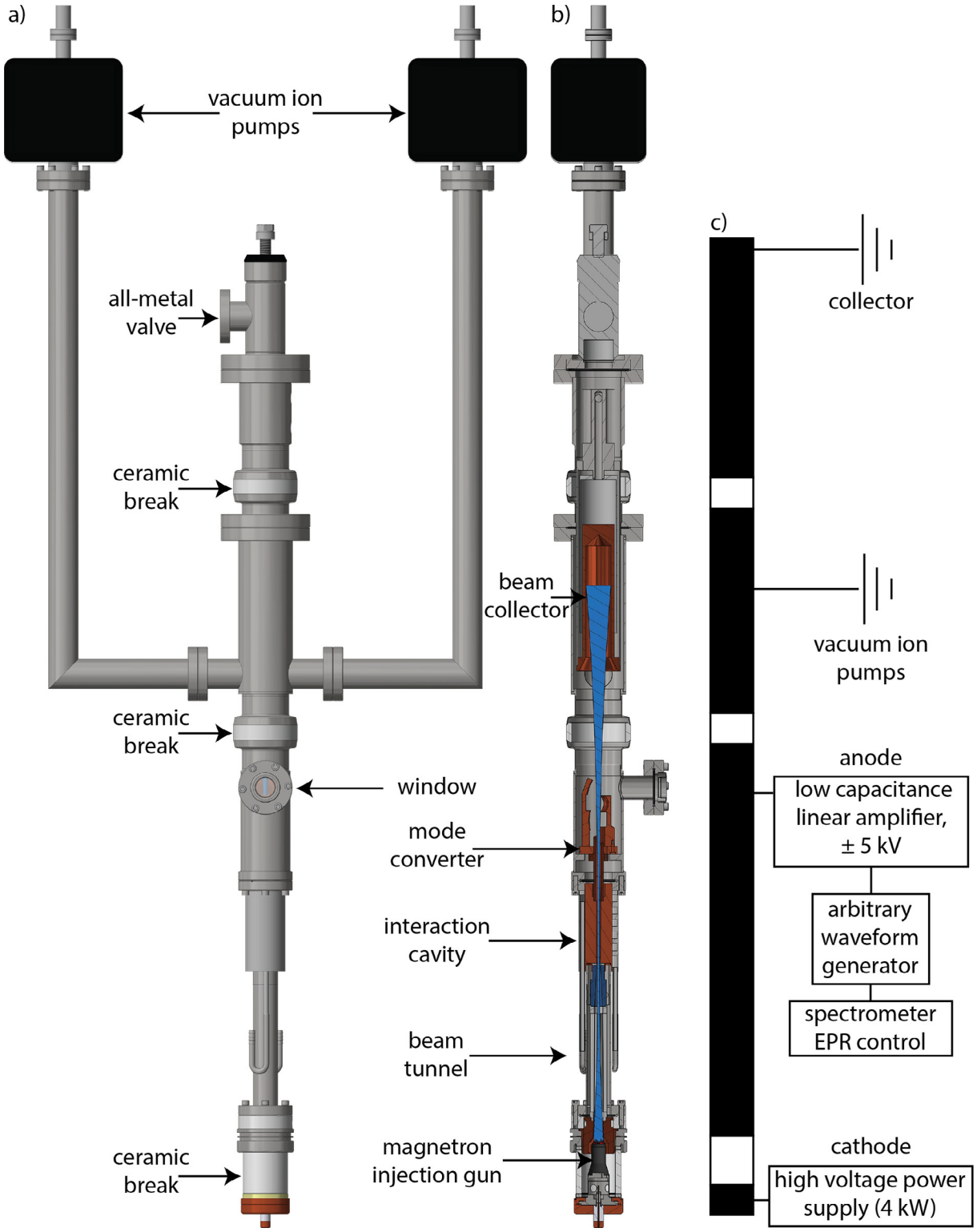

Fig. 2. Schematics of the frequency-agile gyrotron (a) full view and (b) cross section. (c) Electronic schematic showing the anode and cathode connections for frequency agility. Ceramic electrical breaks are shown in white.

the gyrotron body. However, the window has been tested independently of the gyrotron and found to be transparent at 198 GHz. The sapphire is brazed to a Kovar sleeve, which is in turn welded to a 316 stainless steel CF flange to allow for window removal or replacement as needed. The exchangeable window is advantageous compared to welding the window directly to the gyrotron body.

2.7. Alignment apparatus

The purpose of the alignment stage is to adjust the gyrotron position inside the super-conducting magnet to optimize interaction of the electron beam with the interaction cavity. For maximum microwave power output, the electron beam should run parallel to the axis of the interaction cavity, and aligned concentri-

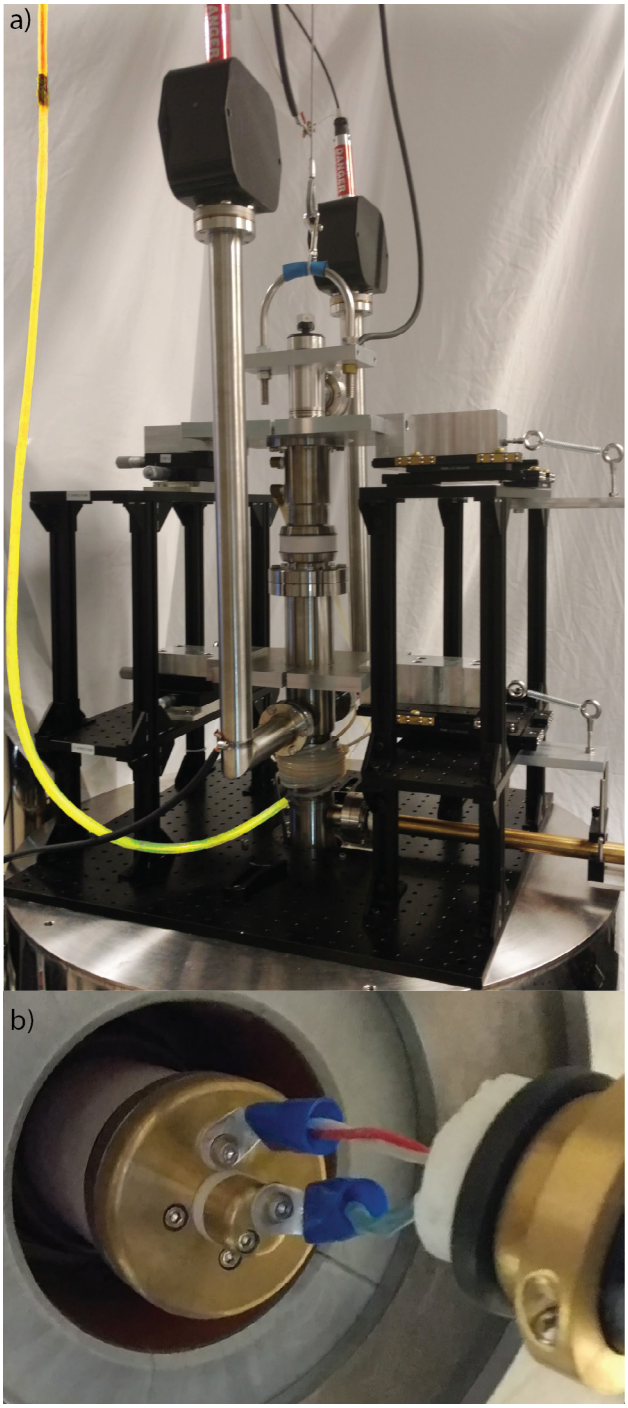

Fig. 3. (a) Photograph of the gyrotron in the magnet. The anode is connected to the low capacitance amplifier by cord highlighted in yellow. (b) Cathode connection to high-voltage power supply. (For interpretation of the references to colour in this figure legend, the reader is referred to the web version of this article.)

cally within the cavity. Misalignment on the scale of fractions of a millimeter lead to drastic reduction in microwave conversion efficiency. The electron beam should overlap with the first radial maximum of the TE_{52q} mode, which is experimentally achieved by changing both the alignment stages and the magnetic field at the electron gun [7]. The gyrotron's alignment apparatus has been optimized since its first installation. The gyrotron was originally held in place by an arm attached to the top of the magnet and

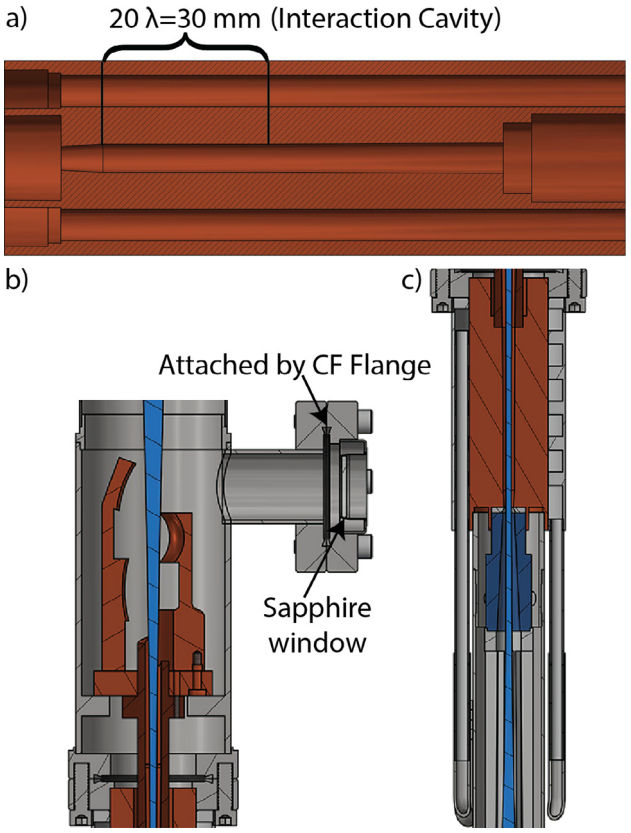

Fig. 4. Schematic of gyrotron (a) cavity (b) internal mode converter, and (c) interaction cavity in context with beam tunnel.

mounted on a table underneath the primary magnet. The top arm was supported by two crossed x-stages such that the cavity's location in the x-y plane could be adjusted in addition to the angle with respect to the electron beam. The bottom stage also held two orthogonal translation stages for alignment, on which a Delrin high-voltage plug was mounted. The high-voltage plug consisted of two brass cylinders fitted with finger-stock separated by a concentric Teflon cylinder. This first design had a number of problems: (i) finger stock was employed for connection of the high-voltage MIG, but often lost electrical connection during the alignment process, (ii) the numbers on the translation stages underneath the magnet could not be read by eye, making precise alignment difficult, and (iii) the high voltage from the power supply occasionally arced to the grounded aluminum table underneath the magnet. For these reasons, a new alignment stage was designed.

The new alignment apparatus features two sets of translation stages mounted to the top of the superconducting magnet, as shown in Fig. 3a. The lower stage support is just above the vacuum extension arms, and the upper stage support is clamped around the top flange of the collector. Alignment is achieved by axial sliding stages shown on the right of the magnet in Fig. 3a. Furthermore, heavy-duty springs accommodate motion when the internal springs of the translation stages are too weak to move the gyrotron.

Although there have been no arcs external to the gyrotron since the plug was replaced, a round Plexiglas shield prevents access to the bottom of the magnet for safety. A second Plexiglas shield sits around the top of the magnet to protect the user from the anode. The upper shield is not shown in Fig. 3 because the glare concealed gyrotron details.

2.8. Fabrication and implementation

The MIG was purchased from Bridge12 Technologies (Framingham, MA). Unless otherwise stated, parts were machined at Washington University in St. Louis from 316 stainless steel or oxygen-free high conductivity (OFHC) copper. Vacuum-tight CF flanges, ceramic breaks, and the all-metal valve were purchased from MDC (Hayward, CA). The internal mode converter was machined at Ramco Machining (Rowley, MA), and the interaction cavity was machined at Midwest Precision Tool and Die (Sioux Falls, SD). The upper beam tunnel was machined in SiC by International Ceramics Engineering (Worchester, MA).

At every welding and brazing step, joints were vacuum tested to ensure proper seals. When all components were complete, each was cleaned meticulously with acetone followed by ethanol to remove machining oils [42]. Prior to operation in the magnet, the gyrotron was baked out under vacuum by wrapping in fiberglass heating tape and covering in aluminum foil. The gyrotron body was heated to 200 °C and the collector was heated to 350 °C for six days. The MIG was then attached for a second vacuum processing session at 100 °C. Subsequently the emitter was activated under a DC potential of 0.3–2.2 V and an AC heater current up to 2.3 A.

3. Results

3.1. Power output and voltage frequency sweeps

The gyrotron microwave power and frequency over a range of 670 MHz (or 4.5 kV) are shown in Fig. 5. To measure power output, a section of corrugated transmission line was removed and a water load of 500 mL was placed in the path of the transmission line at 1 m from the gyrotron window. The water load was stirred continuously and the temperature rise was measured with a thermocouple to determine the microwave power. Microwave frequency was measured with a commercial frequency measurement system (Bridge 12 Technologies, Inc, Framingham, MA). The microwave power output peaked at 27 W, but a frequency span of consistent power at 12–13 W is more desirable for frequency-agile DNP sequences such as electron decoupling. We note that 36 W of power was measured directly at the output window, indicating significant power is lost in the first meter of the transmission line, due to poor mode quality emitted from the gyrotron.

This gyrotron was previously employed in the first utilization of chirped microwave pulses in MAS NMR and concomitant demonstration of electron decoupling [8]. The average NMR linewidth change due to electron decoupling from that study is shown in blue[1] in Fig. 5a [8]. Note that electron decoupling was demonstrated in a bandwidth of constant microwave power output.

The dependence of the microwave frequency on voltage is remarkably linear (Fig. 5b) [34,43]. The frequency measurement system records at a rate of 2 sweeps per second, so this system cannot directly measure the fastest frequency sweeps. Frequency agility is inferred from electron decoupling performance and the observed change in anode voltage [8].

3.2. DNP enhancement profiles

Frequency-stepped DNP enhancement profiles were recorded for Finland trityl radical, N@C_{60} endofullerene, and bcTol-M on the DNP spectrometer (Fig. 6) [44,45]. Two trityl samples at concentrations of 10 mM and 40 mM and bcTol-M at a concentration of 20 mM were characterized; all except the fullerene contained

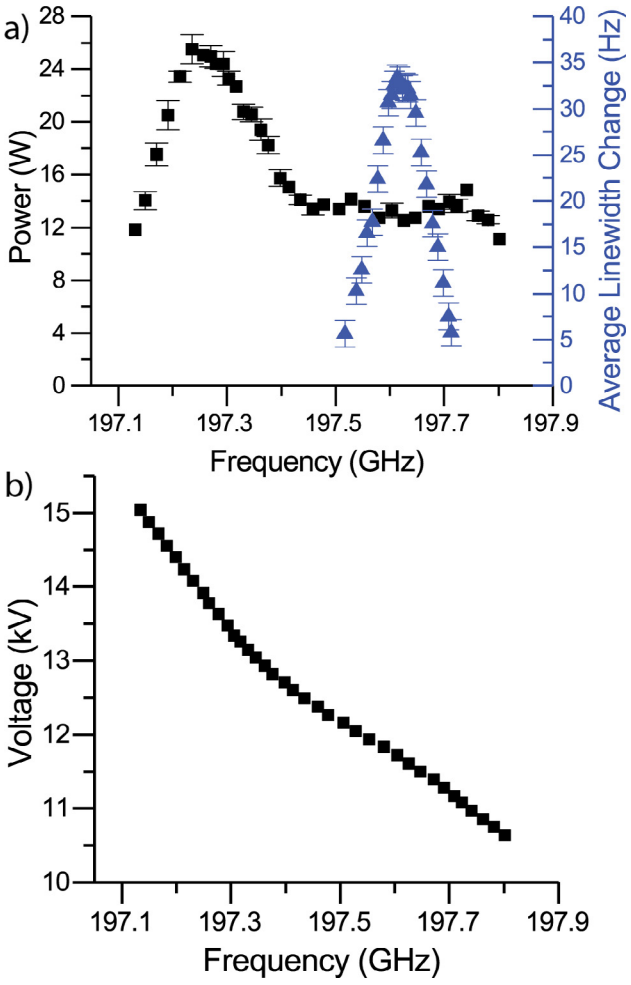

Fig. 5. (a) Gyrotron output power over tuning bandwidth. Power output is stable over a 300 MHz range and present over a 670 MHz (197.13–197.80 GHz) range. Error bars <0.5 W are not shown. Average linewidth change due to electron decoupling (Hz) reproduced with permission from the Journal of the American Chemical Society [8]. (b) Response to change in cathode voltage for the same frequency range.

4 M [^{13}C, ^{15}N] urea in 60% glycerol-d_8, 30% D_2O, and 10% H_2O. The Finland trityl radical was purchased from Oxford Instruments (Abingdon, UK). N@C_{60} endofullerene was prepared and purified following a previously described procedure [46,47]. This useful reference S = 3/2 material is stable at room temperature [48,49]. The final powder contained 170 ppm of N@C_{60} within a cubic lattice of C_{60} (C_{60}:N@C_{60}). ^{13}C DNP NMR was performed on natural abundance ^{13}C nuclei in the C_{60} fullerene. We feature the negative enhancement in this manuscript, but we have observed a positive enhancement 150 MHz away. This confirms the DNP mechanism for N@C_{60} endofullerene is the solid effect.

All profiles were recorded on a custom-built 4-channel NMR DNP MAS probe housing 3.2 mm diameter cylindrical sample containers, or rotors, at a B_0 of 7.05 T. The ^{1}H carrier frequency was 300.184 MHz and the ^{13}C frequency was 75.495 MHz. Specific experimental parameters are given in Table 1. Saturation trains were used to destroy any residual polarization before experiments. The DNP polarization transfer time is defined as τ_{pol}, and the power of the gyrotron was 13–16 W. The temperature was 90 K for all profiles. Profiles were generated by taking individual spectra at varying microwave frequencies and using DMFit [50] to find the areas of resonances recorded with and without microwaves. Each of the areas are plotted as a function of microwave frequency.

[1] For interpretation of color in Fig. 5, the reader is referred to the web version of this article.

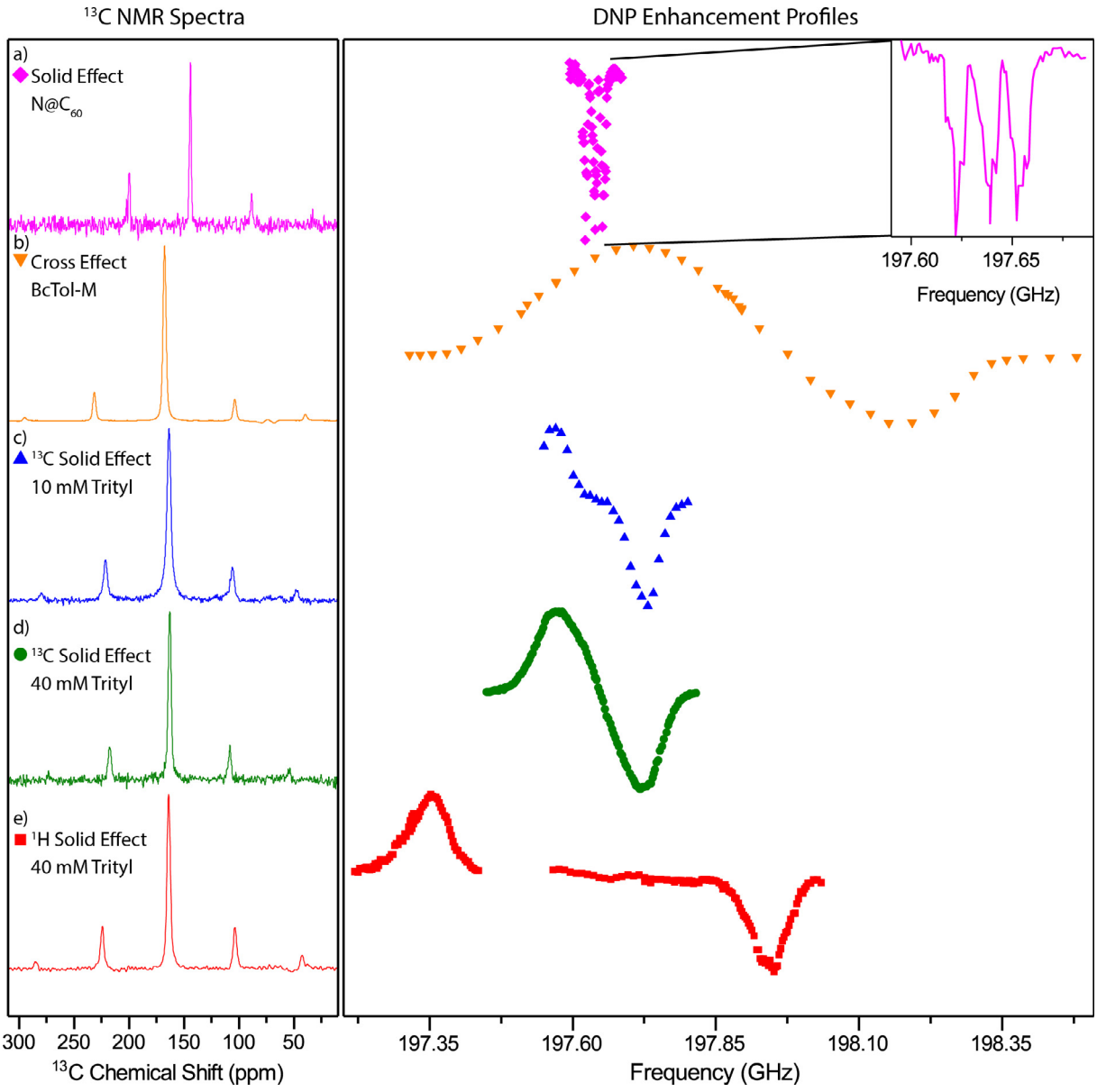

Fig. 6. The left panel shows DNP-enhanced spectra of (a) N@C_{60} endofullerene polarized by solid effect and 4 M [^{13}C, ^{15}N] urea polarized by: (b) cross effect to ^{1}H and CP with bcTol-M at 20 mM, (c) solid effect directly to ^{13}C with trityl at 10 mM, (d) solid effect to ^{13}C with trityl at 40 mM, and (e) solid effect to ^{1}H and CP with trityl at 40 mM. The right panel shows the full enhancement profiles, NMR signal areas vs. microwave irradiation frequency, of each radical. The inset shows a larger scale negative enhancement profile of the N@C_{60} endofullerene.

Table 1
Experimental NMR parameters.

Radical profile	Sequence	ν_{1H} (kHz)	ν_{13C} (kHz)	τ (μs)	ν_{rot} (kHz)	τ_{pol} (s)	Transients	Maximum enhancement	DNP mechanism
bcTol-M	CPMAS	67	83	215	4.6	3	8	342	Cross effect
10 mM trityl	Hahn echo	67	83	250	4.0	7	8	8	Solid effect
40 mM trityl	Hahn echo	67	83	250	4.0	7	4	242	Solid effect/Cross effect
40 mM trityl	CPMAS	67	83	250	4.0	7	4	21	Solid effect
N@C_{60}	Bloch decay	–	83	–	4.2	30	8	1.3	Solid effect

$\nu_{1H} = \omega_{1,1H}/2\pi$ during proton decoupling, $\nu_{13C} = \omega_{1,13C}/2\pi$ during carbon echo pulse, τ = Hahn echo delay time, ν_{rot} = rotation frequency, τ_{pol} = polarization time.

3.3. Spectral purity

The spectral purity is difficult to directly observe with the frequency measurement system due to the instability in the mixer's local oscillator (LO) frequency. As the frequency of the local oscillator changes, so does the difference between the LO signal and the gyrotron output frequency. This results in the appearance of a broadened linewidth as the receiver sweeps across the selected frequency window. However, here we introduce a novel experiment to determine the spectral purity of microwave sources which

should have a broad applicability. The spectral purity can be seen indirectly by overlaying DNP enhancement profile of N@C_{60} with the frequency-shifted EPR signal (Fig. 7). The echo-detected field-sweep EPR spectrum of N@C_{60} was recorded on a 263 GHz Bruker Elexsys E780 puled EPR spectrometer (Bruker, Billerica, MA) using a custom-built resonator. Pulses with a Rabi frequency of 5 MHz were used, the echo delay was set to 600 ns. The superconducting sweep coil of a Bruker Ascent DNP magnet (B_0 = 9.4 T) was used for the field-sweep (sweep rate: 0.01 mT/s). Temperature was regulated at 100 K inside a cryostat (Oxford Instruments). N@C_{60} endofullerene is unique in a sense that the active paramagnetic species is a nitrogen atom in its electronic ground state (S = 3/2) which is trapped inside the highly symmetric cavity of a C_{60} fullerene. This results in an effectively isotropic EPR spectrum with a *g* value close to the free electron and 15.8 MHz hyperfine coupling to the central ^{14}N. If the gyrotron emits a wider range of frequencies over the time course of the experiment (minutes), each peak of the resolved ^{14}N hyperfine triplet in the enhancement profile will be broadened with respect to the EPR spectrum. The enhancement profile of the fullerene, taken together with the EPR spectrum exhibiting 2 MHz broad resonance features, indicates that the spectral bandwidth is a maximum of 7 MHz. We note that the spectral purity is most likely far more narrow at shorter timescales. For instance, we expect the frequency, and therefore phase, to be stable over the 14 μs, 100 MHz microwave chirps employed for electron decoupling [8]. We therefore expect frequency-agile gyrotrons will have the requisite frequency and phase stability to perform chirped microwave pulses also for pulsed DNP transfers.

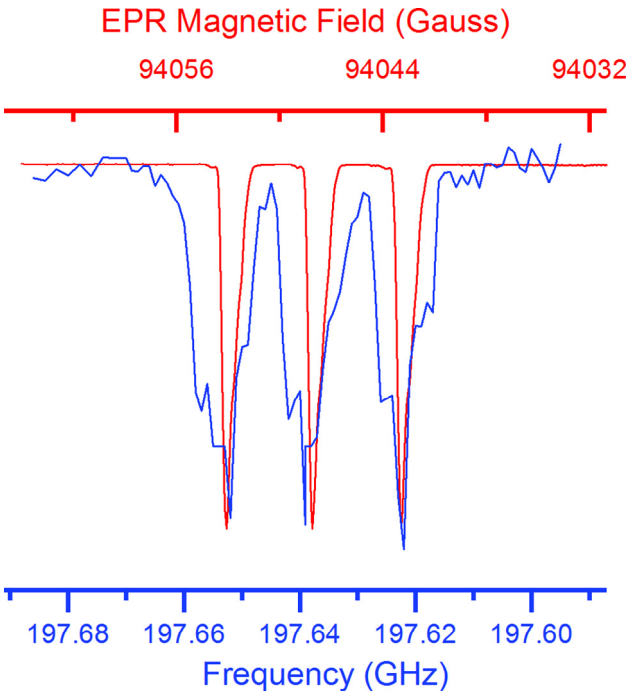

Fig. 7. The top axis and red spectrum show the EPR echo detected field sweep of N@C_{60} endofullerene. The bottom axis and blue spectrum show the enhancement profile of N@C_{60} endofullerene. (For interpretation of the references to colour in this figure legend, the reader is referred to the web version of this article.)

3.4. Microwave duty cycle

The gyrotron is most often operated at a 100% duty cycle, but here we show that the power output can also be gated on a microsecond timescale. This is achieved by quickly jumping the acceleration voltage of the MIG between a potential which yields power emission, and a potential which does not support microwave power generation. In Fig. 8, the duty cycle is synchronized with the rotor period. Rotor period synchronization alone did not yield larger DNP enhancement, however, this on/off microwave control is a useful feature that could be utilized in rotor-synchronized EPR and DNP experiments in the future.

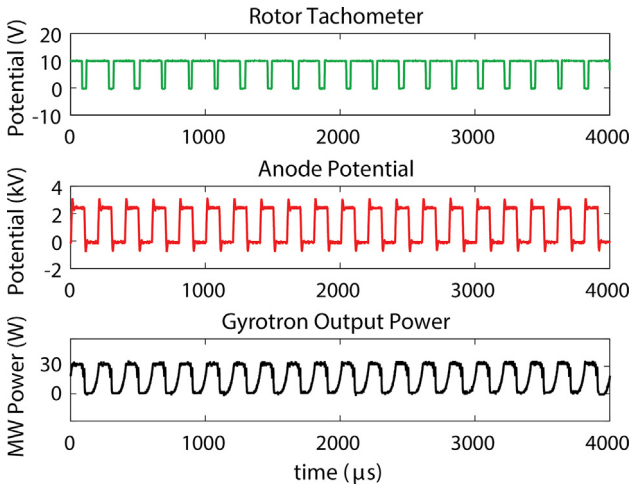

Fig. 8. Anode voltage and microwave duty cycle synchronized to the rotor period.

3.5. Upgrading continuous-wave gyrotrons

Dozens of continuous-wave gyrotrons are already in use for DNP, and many of these gyrotrons could be modified for fast frequency chirps using similar voltage agility techniques to those described here. The anode and cavity body are often electrically connected in gyrotrons currently implemented for DNP, but separated from the collector in order to measure body current. Therefore the anode would need to be connected to a high voltage power supply, rather than connected to ground via a resistor which is the more common arrangement. In principle, such an upgrade would require modifications to the control system and wiring, yet would not require a new gyrotron tube, super conducting magnet, or cathode power supply. We note that the bandwidth of commercially available gyrotrons typically employed for MAS DNP is in the range of 50–130 MHz; not as wide a tuning range as the device we present in this study, but still sufficient to chirp through narrow-line radicals. Such modified devices could also in principle implement the rotor-synchronized microwave gating demonstrated in Fig. 8. If upgrades to DNP spectrometers already in use lead to improved microwave chirping and gating abilities, then the progress of DNP from continuous to pulsed regimes could be substantially accelerated.

4. Conclusion and outlook

Frequency-agile gyrotrons enable a new class of experiments for DNP-NMR spectroscopy. Control of the microwave frequency with our spectrometer allows for chirped microwave pulses in conjunction with MAS NMR. The frequency agility of the gyrotron depends on a low capacitance circuit equipped with an arbitrary waveform generator on the electrically isolated anode. The interaction cavity is long enough to support hybridized axial modes, yielding a continuous microwave power output over a spectral width of 670 MHz at a single magnetic field. The frequency response is linear with respect to voltage, and the microwave power is nearly constant over a 100 MHz tuning range previously employed for electron decoupling. The gyrotron is used to characterize a variety

of radicals including Finland radical trityl, bcTol-M, and N@C_{60} endofullerene. From the fullerene EPR spectrum and DNP enhancement profile, we determine that the spectral bandwidth of the gyrotron is no >7 MHz over a timescale of minutes, but on a microsecond timescale, phase and frequency stability are sufficient for electron decoupling experiments. The gyrotron power emission can be gated with MAS frequency to enable rotor synchronized DNP.

Importantly, we describe how existing DNP spectrometers could be upgraded to permit similar microwave-chirped and microwave-gated control. Improvements in frequency agile gyrotron design will result in higher microwave power levels than the 36 W generated in this device. Applications of frequency agile gyrotrons include electron decoupling and frequency-chirped pulsed DNP. Frequency agile gyrotron technology, if adopted, could usher in a paradigm shift from CW to time domain DNP.

Acknowledgments

This work was supported by the NSF-IDBR (CAREER DBI-1553577), NIH Director's New Innovator Award from the National Institutes of Health (DP2GM119131), and a Small Business Technology Transfer (STTR) grant by the National Science Foundation (STTR 1521314). BC acknowledges funding by the Deutsche Forschungsgemeinschaft (DFG) through Emmy Noether grant CO802/2-1. Further support from the BMRZ is acknowledged. WH and ME acknowledge support from the DFG (Heisenberg Program and Priority Program SPP-1601: New frontiers in sensitivity for EPR spectroscopy) as well as from the VolkswagenStiftung within the funding initiative Integration of Molecular Components in Functional Macroscopic Systems. SS and AJ acknowledge funding from the Icelandic Research Fund (141062051).

References

[1] C. Song, K.-N. Hu, C.-G. Joo, T.M. Swager, R.G. Griffin, TOTAPOL: a biradical polarizing agent for dynamic nuclear polarization experiments in aqueous media, J. Am. Chem. Soc. (2006) 11385–11390, https://doi.org/10.1021/JA061284B.

[2] D. Lee, E. Bouleau, P. Saint-Bonnet, S. Hediger, G. De Paëpe, Ultra-low temperature MAS-DNP, J. Magn. Reson. 264 (2016) 116–124, https://doi.org/10.1016/j.jmr.2015.12.010.

[3] V. Weis, M. Bennati, M. Rosay, J.A. Bryant, R.G. Griffin, High-field DNP and ENDOR with a novel multiple-frequency resonance structure, J. Magn. Reson. 140 (1999) 293–299, https://doi.org/10.1006/jmre.1999.1841.

[4] A.B. Barnes, E. Markhasin, E. Daviso, V.K. Michaelis, E.A. Nanni, S.K. Jawla, et al., Dynamic nuclear polarization at 700MHz/460GHz, J. Magn. Reson. 224 (2012) 1–7, https://doi.org/10.1016/j.jmr.2012.08.002.

[5] L.R. Becerra, G.J. Gerfen, R.J. Temkin, D. Singel, R.G. Griffin, Dynamic nuclear polarization with a cyclotron resonance maser at 5 T, Phys. Rev. Lett. 71 (1993) 3561–3564, https://doi.org/10.1103/PhysRevLett. 71.3561.

[6] Y. Matsuki, T. Idehara, J. Fukazawa, T. Fujiwara, Advanced instrumentation for DNP-enhanced MAS NMR for higher magnetic fields and lower temperatures, J. Magn. Reson. 264 (2016) 107–115, https://doi.org/10.1016/j.jmr.2016.01.022.

[7] A.B. Barnes, E.A. Nanni, J. Herzfeld, R.G. Griffin, R.J. Temkin, A 250 GHz gyrotron with a 3 GHz tuning bandwidth for dynamic nuclear polarization, J. Magn. Reson. 221 (2012) 147–153, https://doi.org/10.1016/j.jmr.2012.03.014.

[8] E.P. Saliba, E.L. Sesti, F.J. Scott, B.J. Albert, E.J. Choi, N. Alaniva, et al., Electron decoupling with dynamic nuclear polarization in rotating solids, J. Am. Chem. Soc. 139 (2017) 6310–6313, https://doi.org/10.1021/jacs.7b02714.

[9] M. Garwood, L. DelaBarre, The return of the frequency sweep: designing adiabatic pulses for contemporary NMR, J. Magn. Reson. 153 (2001) 155–177, https://doi.org/10.1006/jmre.2001.2340.

[10] Ê. Kupce, R. Freeman, Optimized adiabatic pulses for wideband spin inversion, J. Magn. Reson. Ser. A. 118 (1996) 299–303, https://doi.org/10.1006/jmra.1996.0042.

[11] I. Kaminker, R.P. Barnes, S. Han, Arbitrary waveform modulated pulse EPR at 200 GHz, J. Magn. Reson. 279 (2017) 81–90, https://doi.org/10.1016/j.jmr.2017.04.016.

[12] S.K. Jain, G. Mathies, R.G. Griffin, Off-resonance NOVEL, J. Chem. Phys. 147 (2017).

[13] V.S. Bajaj, C.T. Farrar, M.K. Hornstein, I. Mastovsky, J. Vieregg, J.A. Bryant, et al., Dynamic nuclear polarization at 9T using a novel 250GHz gyrotron microwave source, J. Magn. Reson. 160 (2003) 85–90, https://doi.org/10.1016/S1090-7807(02)00192-1.

[14] A. Henstra, T.-S. Lin, J. Schmidt, W.T. Wenckebach, High dynamic nuclear polarization at room temperature, Chem. Phys. Lett. 165 (1990) 6–10.

[15] A. Bornet, J. Milani, B. Vuichoud, A.J. Perez Linde, G. Bodenhausen, S. Jannin, Microwave frequency modulation to enhance dissolution dynamic nuclear polarization, Chem. Phys. Lett. 602 (2014) 63–67, https://doi.org/10.1016/j.cplett.2014.04.013.

[16] Y. Hovav, A. Feintuch, S. Vega, D. Goldfarb, Dynamic nuclear polarization using frequency modulation at 3.34 T, J. Magn. Reson. 238 (2014) 94–105, https://doi.org/10.1016/j.jmr.2013.10.025.

[17] T.V. Can, R.T. Weber, J.J. Walish, T.M. Swager, R.G. Griffin, Frequency-Swept Integrated Solid Effect, Angew. Chemie - Int. Ed. 56 (2017) 6744–6748, https://doi.org/10.1002/anie.201700032.

[18] S. Un, T.F. Prisner, R.T. Weber, M.J. Seaman, K.W. Fishbein, A.E. McDermott, et al., Pulsed dynamic nuclear polarization at 5 T, Chem. Phys. Lett. 189 (1992) 54–59, https://doi.org/10.1016/0009-2614(92)85152-Z.

[19] L.R. Becerra, G.J. Gerfen, B.F. Bellew, J.A. Bryant, D.A. Hall, S.J. Inati, et al., A spectrometer for dynamic nuclear-polarization and electron-paramagnetic-resonance at high-frequencies, J. Magn. Reson. Ser. A. 117 (1995) 28–40.

[20] E.A. Nanni, S.M. Lewis, M.A. Shapiro, R.G. Griffin, R.J. Temkin, Photonic-band-gap traveling-wave gyrotron amplifier, Phys. Rev. Lett. 111 (2013) 1–5, https://doi.org/10.1103/PhysRevLett. 111.235101.

[21] S. Alberti, F. Braunmueller, T.M. Tran, J. Genoud, J.P. Hogge, M.Q. Tran, et al., Nanosecond pulses in a THz gyrotron oscillator operating in a mode-locked self-consistent Q-switch regime, Phys. Rev. Lett. 111 (2013) 205101.

[22] A.C. Torrezan, S.T. Han, I. Mastovsky, M.A. Shapiro, J.R. Sirigiri, R.J. Temkin, et al., Continuous-wave operation of a frequency-tunable 460-GHz second-harmonic gyrotron for enhanced nuclear magnetic resonance, IEEE Trans. Plasma Sci. 38 (2010) 1150–1159, https://doi.org/10.1109/tps.2010.2046617.

[23] J.H. Booske, R.J. Dobbs, C.D. Joye, C.L. Kory, G.R. Neil, G.S. Park, et al., Vacuum electronic high power terahertz sources, IEEE Trans. Terahertz Sci. Technol. 1 (2011) 54–75, https://doi.org/10.1109/TTHZ.2011.2151610.

[24] G.S. Nusinovich, Gyrotron oscillators for controlled fusion experiments, in: Introd. to Phys. Gyrotrons, The John Hopkins University Press, 2004, pp. 215–238.

[25] D.T. Edwards, Y. Zhang, S.J. Glaser, S. Han, M.S. Sherwin, Phase cycling with a 240 GHz, free electron laser-powered electron paramagnetic resonance spectrometer, Phys. Chem. Chem. Phys. 15 (2013) 5707, https://doi.org/10.1039/c3cp44492a.

[26] C.D. Joye, A.M. Cook, J.P. Calame, D.K. Abe, A.N. Vlasov, I.A. Chernyavskiy, et al., Demonstration of a high power, wideband 220-GHz traveling wave amplifier fabricated by UV-LIGA, IEEE Trans. Electron Devices. 61 (2014) 1672–1678, https://doi.org/10.1109/TED.2014.2300014.

[27] Y.M. Shin, L.R. Barnett, N.C. Luhmann, Phase-shifted traveling-wave-tube circuit for ultrawideband high-power submillimeter-wave generation, IEEE Trans. Electron Devices. 56 (2009) 706–712, https://doi.org/10.1109/TED.2009.2015404.

[28] C.S. Kou, Q.S. Wang, D.B. McDermott, N.C. Luhmann, K.R. Chu, A.T. Lin, High-power harmonic Gyro-TWT's—Part I: linear theory and oscillation study, IEEE Trans. Plasma Sci. 20 (1992) 155–162, https://doi.org/10.1109/27.142815.

[29] E.N. Comfoltey, M.A. Shapiro, J.R. Sirigiri, R.J. Temkin, Design of an overmoded W-band TWT, 2009 IEEE Int, Vac. Electron. Conf. IVEC 2009 (2009) 127–128, https://doi.org/10.1109/IVELEC.2009.5193391.

[30] C.D. Joye, M.A. Shapiro, J.R. Sirigiri, R.J. Temkin, Demonstration of a 140-GHz 1-kW confocal gyro-traveling-wave amplifier, IEEE Trans. Electron Devices. 56 (2009) 818–827, https://doi.org/10.1109/TED.2009.2015802.

[31] D.E.M. Hoff, B.J. Albert, E.P. Saliba, F.J. Scott, E.J. Choi, M. Mardini, et al., Frequency swept microwaves for hyperfine decoupling and time domain dynamic nuclear polarization, Solid State Nucl. Magn. Reson. 72 (2015) 79–89, https://doi.org/10.1016/j.ssnmr.2015.10.001.

[32] T. Idehara, E.M. Khutoryan, Y. Tatematsu, Y. Yamaguchi, A.N. Kuleshov, O. Dumbrajs, et al., High-speed frequency modulation of a 460-GHz gyrotron for enhancement of 700-MHz DNP-NMR spectroscopy, J. Infrared, Millimeter, Terahertz Waves. 36 (2015) 819–829, https://doi.org/10.1007/s10762-015-0176-2.

[33] D. Yoon, M. Soundararajan, P. Cuanillon, F. Braunmueller, S. Alberti, J.P. Ansermet, Dynamic nuclear polarization by frequency modulation of a tunable gyrotron of 260 GHz, J. Magn. Reson. 262 (2016) 62–67, https://doi.org/10.1016/j.jmr.2015.11.008.

[34] S. Alberti, J.P. Ansermet, K.A. Avramides, F. Braunmueller, P. Cuanillon, J. Dubray, et al., Experimental study from linear to chaotic regimes on a terahertz-frequency gyrotron oscillator, Phys. Plasmas. 19 (2012), https://doi.org/10.1063/1.4769033.

[35] B.J. Albert, S.H. Pahng, N. Alaniva, E.L. Sesti, P.W. Rand, E.P. Saliba, et al., Instrumentation for cryogenic magic angle spinning dynamic nuclear polarization using 90 L of liquid nitrogen per day, J. Magn. Reson. 283 (2017) 71–78, https://doi.org/10.1016/j.jmr.2017.08.014.

[36] E.L. Sesti, N. Alaniva, P.W. Rand, E.J. Choi, B.J. Albert, E.P. Saliba, et al., Magic angle spinning NMR below 6 K with a computational fluid dynamics analysis of fluid flow and temperature gradients, J. Magn. Reson. (2017), https://doi.org/10.1016/j.jmr.2017.11.002.

[37] J. Schaefer, R.A. McKay, Multi-Tuned Single Coil Transmission Line Probe for Nuclear Magnetic Resonance Spectrometer, 1999.

[38] S.J. Kim, L. Cegelski, D. Stueber, M. Singh, E. Dietrich, K.S.E. Tanaka, et al., Oritavancin exhibits dual mode of action to inhibit cell-wall biosynthesis in staphylococcus aureus, J. Mol. Biol. 377 (2008) 281–293, https://doi.org/10.1016/j.jmb.2008.01.031.

[39] M. Rosay, L. Tometich, S. Pawsey, R. Bader, R. Schauwecker, M. Blank, et al., Solid-state dynamic nuclear polarization at 263 GHz: spectrometer design and experimental results, Phys. Chem. Chem. Phys. 12 (2010) 5741–5751, https://doi.org/10.1039/c003685b.
[40] J.L. Doane, Propagation and mode coupling in corrugated and smooth-wall circular waveguides, Infrared Millim. Waves 13 (1985) 123–170.
[41] S.N. Vlasov, L.I. Zagryadskaya, M.I. Petelin, Transformation of a whispering gallery mode, propagating in a circular waveguide, into a beam of waves, Radio Eng. Electron. Phys. 10 (1975) 14–17.
[42] S.V. Kagwade, C.R. Clayton, D. Chidambaram, G.P. Halada, Photochemical breakdown of acetone on copper, Electrochim. Acta. 46 (2001) 2337–2342, https://doi.org/10.1016/S0013-4686(01)00359-0.
[43] B. Piosczyk, A. Arnold, G. Dammertz, M. Kuntze, G. Michel, O.S. Lamba, et al., Step-frequency operation of a coaxial cavity from 134 to 169.5 GHz, IEEE Trans. Plasma Sci. 28 (2000) 918–923, https://doi.org/10.1109/27.887753.
[44] A.P. Jagtap, M.-A. Geiger, D. Stöppler, M. Orwick-Rydmark, H. Oschkinat, S.T. Sigurdsson, bcTol: a highly water-soluble biradical for efficient dynamic nuclear polarization of biomolecules, Chem. Commun. 52 (2016) 7020–7023, https://doi.org/10.1039/C6CC01813K.
[45] M.-A. Geiger, A.P. Jagtap, M. Kaushik, B. Corzilius, H. Oschkinat, S.T. Sigurdsson, Efficiency of water-soluble nitroxide biradicals for dynamic nuclear polarization in rotating solids at 9.4 T: bcTol-M and cyolyl-TOTAPOL as new polarizing agents, Manuscr. Prep. (2017).
[46] T. Almeida Murphy, T. Pawlik, A. Weidinger, M. Höhne, R. Alcala, J.M. Spaeth, Observation of atomlike nitrogen in nitrogen-implanted solid C60, Phys. Rev. Lett. 77 (1996) 1075–1078, https://doi.org/10.1103/PhysRevLett. 77.1075.
[47] P. Jakes, K.-P. Dinse, C. Meyer, W. Harneit, A. Weidinger, Purification and optical spectroscopy of N@C60, Phys. Chem. Chem. Phys. 5 (2003) 4080, https://doi.org/10.1039/b308284a.
[48] C. Meyer, W. Harneit, B. Naydenov, K. Lips, A. Weidinger, N@C60 and P@C60 as Quantum Bits, Appl. Magn. Reson. 27 (2004) 123–132, https://doi.org/10.1007/BF03166307.
[49] M. Eckardt, R. Wieczorek, W. Harneit, Stability of C60 and N@C60 under thermal and optical exposure, Carbon N. Y. 95 (2015) 601–607, https://doi.org/10.1016/j.carbon.2015.08.073.
[50] D. Massiot, F. Fayon, M. Capron, I. King, S. Le Calvé, B. Alonso, et al., Modelling one- and two-dimensional Solid State NMR spectra, Magn. Reson. Chem. 40 (2002) 70–76, https://doi.org/10.1002/mrc.984.